Title: **Nuclear Abl Drives Extracellular-Vesicle Transfer of miR-34c to Induce Bystander Effects of Radiation**

Affiliation: Department of Medicine, Division of Hematology-Oncology, University of California, San Diego, School of Medicine, 9500 Gilman Drive, La Jolla, CA 92093-0644

Authors: Shubhra Rastogi, Amini Hwang, Josolyn Chan and Jean Y J Wang*

Keywords: **DDR, Extracellular Vesicles, γH2AX, microRNA, NAC, Reactive Oxygen Species**, **Roscovitine**

Financial Support: **USA National Cancer Institute Grant (R01CA043054) to JYJW**

***Corresponding author:**

Jean Y J Wang, PhD

Distinguished Professor of Medicine

George Palade Laboratories, Room 256

University of California, San Diego

9500 Gilman Drive

La Jolla, CA 92093-0644

Telephone: 1-(858)-534-6253

Email: jywang@ucsd.edu

The authors declare no conflicts of interest

Total number of Figures: 4

Total number of extended Figures: 14

Ionizing radiation (IR) activates DNA damage response (DDR) that includes induction of bystander effects (BE) in cells not directly targeted by radiation. How DDR pathways in irradiated cells stimulate BE in non-targeted cells is mostly unknown. We show here that extracellular vesicles from irradiated cells (EV-IR) induce reactive oxygen species (ROS), increase γH2AX and Rad51-foci, and reduce clonogenic survival when taken up by un-irradiated cells. Among the direct effects of IR is Abl nuclear accumulation; interestingly, EV-IR from Abl NLS-mutated cells could not induce BE, and restoration of nuclear Abl rescued that defect. Extending our previous finding that Abl stimulates miR-34c expression in DDR, we found that that nuclear Abl also increased miR-34c levels in EV-IR. Co-expression of miR-34c-minigene and activated Abl led to the production, without irradiation, EV-miR-34c with BE-inducing activity. Furthermore, EV-IR from miR34-knockout cells could not induce ROS and raised γH2AX levels to lesser extent than those from miR34-wild type cells. These results establish a novel role for nuclear Abl and miR-34c in transmitting DNA damage response from directly irradiated cells to un-irradiated bystander cells.

In multicellular organisms, ionizing radiation (IR) damages DNA to activate a wide range of DDR not only in directly irradiated cells but also in neighboring or distant cells not targeted by IR. The non-target or bystander effects (BE) of IR occurs when irradiated cells secrete soluble factors and extracellular vesicles

(EV) to propagate the damage signal to naïve, non-irradiated cells[1-3]. It was reported that DDR master regulators, i.e., ATM and p53, are required for irradiated cells to secrete bystander effectors[4,5], however, how other DDR pathways stimulate BE is mostly unknown. IR stimulates nuclear accumulation and activation of Abl tyrosine kinase to regulate transcription, DNA repair and microRNA processing[6-10]. Because EV can transfer microRNAs between cells[11-14], we investigated the role of nuclear Abl and its regulated microRNA, miR-34c, in EV-mediated bystander effects of radiation.

We isolated extracellular vesicles (EV) from media conditioned by immortalized mouse embryo fibroblasts (MEFs) and avoided EV from serum by switching cells into serum-free media before irradiation (extended Fig. E1A)[15,16]. We found similar size distributions, particle concentrations and total proteins among multiple independent EV preparations from non-irradiated (EV-C) or irradiated (EV-IR) MEFs and HEK293T cells (extended Figs E1B, C; E9D, E; E11A-D; E13A). We also found that naïve non-irradiated MEFs (responders) internalize EV-C and EV-IR to comparable levels (extended Fig. E1D, E). Thus, IR does not grossly alter the production or the uptake of EV.

Inhibition of colony formation is both a direct and a bystander effect of ionizing radiation (Fig. 1A, B)[1] , as media conditioned by irradiated MEFs (CM-IR) inhibits colony formation when transferred to responder MEFs (Fig. 1A, B). We found that the EV-pellet fraction of CM-IR retained more of this colony-inhibitory activity than the supernatant fraction (Fig. 1A, B, EV-IR). Titration experiments showed EV-IR to inhibit colony formation in a dose-dependent manner, reaching

saturation at EV-protein levels that approximated a particle/responder cell ratio of 1000 (Fig. 1E, F), while EV-C did not elicit such dose-response (Fig. 1C, D). While direct irradiation of responder MEFs increased p21Cip1 mRNA and protein (extended Fig. E2), induced cell cycle arrest (extended Fig. E3) and senescence (extended Fig. E4), we found that EV-IR did not induce p21Cip1 (extended Fig. E2), cell-cycle arrest (extended Fig. E3), or senescence (extended Fig. E4). Although immortal, the responder MEFs formed colonies at a low frequency (~5%), and EV-IR inhibited the colony-forming activity of this small fraction of responder cells without inducing cell cycle arrest or senescence in the general population that internalized EV-IR (extended Fig. E1D, E).

EV-IR, but not EV-C, also caused dose-dependent increase in the production of reactive oxygen species (ROS) (Fig. 2A, B), which is another direct and bystander effect of IR[17]. The anti-oxidant N-Acetyl Cysteine (NAC) neutralized EV-IR-induced ROS increase (Fig. 2A, EV-IR+NAC) and interfered with the colony inhibitory activity of EV-IR (Fig. 2C), suggesting that ROS was a major albeit not the only contributing factor to colony inhibition. Treatment with Proteinase K or RNase A[16-18] did not abolish the colony-inhibitory or the ROS-inducing activity of EV-IR (extended Fig. E5), indicating that the bystander inducers were sequestered within EV-IR.

Another bystander effect of radiation is the induction of DNA damage in non-irradiated cells[19]. We found that addition of EV-IR, but not EV-C, unto responder cells increased γH2AX (Fig. 2D, extended Fig. E6B) and Rad51-foci (Fig. 2E,F, extended Fig. E7). Although NAC interfered with EV-IR-induced ROS,

it did not block EV-IR-induced γH2AX increase (Fig. 2D). Because EV-IR caused γH2AX and Rad51 foci to increase in only a subpopulation of responder cells (extended Fig. E6B, Fig. 2F, extended Fig. E7), and because γH2AX and Rad51 foci can occur during DNA replication[20,21], we tested and found that the Cdk-inhibitor Roscovitine (Rosc) could prevent EV-IR from increasing γH2AX (extended Fig. E8). Thus, EV-IR might cause replication stress to induce bystander DNA damage

To determine the function of nuclear Abl in DDR, we generated the *Abl-μNLS* allele in mouse germline by mutating the three nuclear localization signals (NLS) in the Abl protein (Fig. 3A)[7,22]. Although IR did not induce nuclear accumulation of Abl-μNLS (Fig. 3B), it increased ROS and γH2AX in *Abl-μNLS* MEFs (Fig. 3C, D) and decreased colony formation (extended Fig. E9A). Thus, nuclear Abl is not essential to the direct effects of radiation in mouse embryo fibroblasts. In contrast, we found that EV from irradiated *Abl-μNLS* MEFs (μEV-IR) (extended Fig. E9D, E) did not induce ROS (Fig. 3E), increase γH2AX (Fig. 3F), nor inhibit colony formation (extended Fig. E9F) in responder MEFs (*Abl-wt)*. We also found that the levels of γH2AX in directly irradiated MEFs were significantly higher than those in EV-IR-treated responder MEFs (extended Fig. E9B & E9C); this could explain why EV-IR did not induce cell cycle arrest. To rescue the μEV-IR defects, we stably expressed Abl^{WT} (or $Abl^{\mu NLS}$ as control) in *Abl-μNLS* MEFs and showed that IR induced nuclear accumulation of Abl^{WT} but not $Abl^{\mu NLS}$ (extended Fig. E10A-C). Expression of Abl^{WT} or $Abl^{\mu NLS}$ did not affect the direct effects of IR in *Abl-μNLS* MEFs (extended Fig. 10D-F); however, Abl^{WT}

but not Abl$^{\mu NLS}$ restored the ability of μEV-IR to increase ROS and γH2AX in responder MEFs (extended Fig. 11E, F). Together, these results establish that nuclear entry of Abl is dispensable to the direct effects of radiation but it is required for irradiated cells to produce BE-inducing EV-IR.

IR induces the expression of many miRs in directly irradiated cells[23], with Abl stimulating *pri-miR34b/c* processing to *pre-miR-34b* and *pre-miR-34c*[9]. In keeping with those results, we found higher levels of miR-34c in directly irradiated *Abl-wt* than *Abl-μNLS* MEFs (Fig. 4A). We also found that EV-IR contained higher levels of miR-34c than EV-C (Fig. 4B), but μEV-IR did not contain higher miR-34c levels than μEV-C (Fig. 4B). In responder cells, miR-34c levels increased only after treatment with EV-IR but not with EV-C, μEV-C or μEV-IR (Fig. 4C). Re-expression of Abl^{WT} in *Abl-μNLS* MEFs restored miR-34c increase in μEV-IR, and in responder cells treated with μEV-IR (extended Fig. E12A-C). These results showed that nuclear Abl stimulated not only the expression but also the inclusion of miR-34c in EV-IR for transfer into responder cells.

To determine if miR-34c is an inducer of BE, we co-expressed miR-34c-minigene with a constitutively activated Abl kinase (AblPPn) (Fig. 4D) in HEK293T cells. The miR-34c-minigene raised miR-34c levels in transfected cells (Fig. 4E) and in EV isolated from the media of those transfected cells (Fig. 4F, extended Fig. E13A). Co-expression with AblPPn further increased the intracellular and the EV levels of miR-34c (Fig. 4E, F). When added to responder MEFs, both EV-miR-34c and EV-miR-34c+AblPPn increased the intracellular

levels of miR-34c (Fig. 4G), inhibited colony formation (Fig. 4H, extended Fig. E13B), induced ROS (Fig. 4I, extended Fig. E13C, D) and the extent of those effects correlated with the levels of miR-34c in EV and in EV-treated responder cells (Fig. 4F,G). With γH2AX, only EV-miR-34c+AblPPn significantly increased its levels above background (Fig. 4J, extended Fig. E13E, F), indicating that higher levels of miR34c might be required to cause DNA damage. To determine if miR-34c is necessary to cause BE, we isolated EV-IR from media conditioned by miR34-family (a, b, c) triple knockout MEFs (miR34^{TKO}) and wild-type littermate MEFs (miR34^{WT})[24]. We found that EV-IR-miR34^{TKO} failed to induce ROS in responder MEFs (*Abl-wt*) (Fig. 4K, extended Fig. E13G, H). EV-IR-miR34^{TKO} treated MEFs show γH2AX staining but to significantly lower levels than EV-IR-miR34^{WT} (Fig. 4L, extended Fig. E13I, J). These results showed that miR-34c and related family members (miR-34a, miR-34b) are required for EV-IR-induced ROS and they contribute to γH2AX increase in responder cells.

Previous studies have identified a number of pro-mitogenic genes as miR-34 targets[25, 26]. We tested three such targets and found in responder cells that EV-IR treatment did not reduce *Pdgfra* or *Pdgfrb* but significantly reduced *Myc* RNA (extended Fig. E14); this *Myc* reduction might account for the colony inhibitory activity of EV-IR and EV-miR-34c. Our finding that NAC reduced ROS but not γH2AX suggests that these EV-IR effects may involve multiple miR-34c target genes. Computational analyses have predicted hundreds of miR-34c targets that may be involved in the observed increase in ROS or γH2AX. It is possible that miR-34c triggers a cascade of gene expression alterations or this

microRNA may collaborate with other EV-delivered factors to increase ROS and γH2AX. Our findings that nuclear Abl is essential for irradiated cells to produce EV-IR with ROS- and γH2AX-inducing activities, but the miR34-family is essential only for the ROS-inducing activity suggest that EV-IR must contain other nuclear-Abl-dependent DNA damage-inducers that remain to be identified.

MATERIALS & METHODS

Cell Lines: Fibroblasts were derived from *Abl*$^{+/+}$ (*Abl-wt*) or littermate *Abl*$^{\mu/\mu}$ (*Abl-μNLS)* mouse embryos[22]. The *Abl-μNLS* allele was generated by knock-in mutations to substitute the eleven lysines and arginines in the three nuclear localization signals (NLS) with glutamine[7]. The *Abl-wt* and *Abl-μNLS* mouse embryo fibroblasts (MEFs) were immortalized by serial passages, and these MEFs do not express p53. Primary, non-immortalized, MEFs from *miR-34a, b, c*-triple knockout mice (miR34^{TKO}) and wild-type littermates (miR34^{WT})[24] were irradiated between passages 3 and 6. MEFs and HEK293T cells (Thermo Fisher Scientific) were cultured in DMEM high glucose media with 10% fetal bovine serum (FBS) and antibiotics.

Irradiation: Cells were exposed to 10 Gy of gamma-irradiation using Mark I model 50 irradiator with Cesium 137 isotope as source (Maker: J.L. Shepherd & Associates).

Isolation of Extracellular Vesicle (EV): To avoid EV from fetal bovine serum (FBS), cells were switched to FBS-free media with 1% BSA two hours before irradiation. At 24 hours after irradiation, the media were collected for EV isolation

by differential ultracentrifugation as previously described[15] (extended Fig. E1A). The pelleted EV fractions were washed and re-suspended in PBS and stored in aliquots at -80° C. For isolation of EV from HEK293T cells, supernatant collected after the 2000g spin was filtered through a 0.45-micron filter (Corning) before continuing onto the next steps of ultracentrifugation. Protein content of EV was determined by the Lowry method.

Nanoparticle Track Analysis: Nanosight LM-10HS was used to determine the number and the size distribution of particles in the EV fractions. Each EV preparation was analyzed in triplicates as previously described[27].

Extracellular Vesicle Uptake: The EV pellets were incubated with PKH26, a fluorescent membrane-binding dye (Sigma Aldrich, St. Louis) for 5min at room temperature, followed by addition of 1% BSA, and then centrifuged at 100,000g for 70min to isolate PKH26-labeled EV[28]. Responder MEFs were incubated with PKH26 in PBS (phosphate buffered saline), or PKH26-labeled EV-C or PKH26-labeled EV-IR (25µg each). After 3 or 24 hours, cells were fixed with 4% para-formaldehyde (PFA) for 20min at room temperature and counterstained with Hoechst 33342. Cells were viewed using an Olympus FV1000 Spectral Confocal microscope. No fluorescence was detected in cells incubated with PKH in PBS. Using FIJI (ImageJ), we measured the PKH26 mean gray values from at least 200 cells per treatment and calculated the mean and standard deviations. The number of PKH26-positive cells was counted by eye, and percentages were calculated from PKH26-positive cells over total number of nuclei.

Colony Formation Assay: Responder cells (*Abl-wt* MEFs) were seeded at 1000 cells per 6-cm plate. Media was changed to 1% BSA without FBS before incubation with EV. After 24 hours, cells were switched back to media with 10% FBS and cultured for 15 days with media refreshed every other day. The colonies were fixed with 100% methanol and stained with 0.05% crystal violet. Excess dye was removed & plates were left to dry over-night. Cluster of more than 50 cells were considered as colonies. Survival fraction was calculated as colonies/cells seeded with the survival fraction in PBS treated plates set to 1. Images of the colonies were acquired using Alpha imager HP System.

Reactive Oxygen Species (ROS) Assay: ROS was measured using the ROS-ID kit (Enzo Life Sciences, Farmingdale) according to manufacturer's protocol. Live cells were also stained with Cell Tracker Red (CTR) (Molecular Probe) as a control for cell volume. Responder cells were seeded into chamber slides, incubated with EV in serum-free media containing 1% BSA for 24 hours, then stained with CTR and DCFDA. Immediately after dye addition, live cell images were captured using an Olympus FV1000 Spectral Confocal Microscope for CTR (Channel 3) & DCFDA (Channel 1). FIJI (ImageJ) software was used to create masks of cells from channel 3 (CTR), and then the masks were transferred onto channel 1 (DCFDA). The mean gray values were measured within the masks, and the DCFDA/CTR mean gray value ratio was calculated for each mask. Ratios of at least 200 cells were calculated per sample per experiment. The DCFDA/CTR ratios of individual cells from a representative experiment are shown in extended Fig. E6A.

Immunofluorescence: Acid-washed coverslips stored in 100% ethanol were placed in 24-well plates and approximately 20,000 MEFs were seeded per well. After incubation with EV for 24 hours in serum-free media containing 1% BSA, cells were fixed in 4% PFA for 15 min, washed with 0.02% Tween-20 in Tri-buffered saline (TBS) twice (5 min each), permeablized with 1% Triton X-100 in TBS for 15 min and then blocked with 5% BSA for 30 min at room temperature. The coverslips were incubated with primary antibody for 1 hour in 37°C: anti-Abl (8E9) (6μg/ml) from ThermoFisher Scientific, anti-phospho-Ser139-H2AX (1/400) from Cell Signaling, anti-RAD51 (1/50) from Santa Cruz. Coverslips were washed twice with 0.02% Tween-20 in TBS twice (5 min each) and then incubated with ALEXA fluor-488 (Invitrogen)-chicken anti-mouse (1/500) or ALEXA fluor-594 (Invitrogen)-donkey anti-rabbit (1/500) at 37°_C for 30 min. Nuclei were stained with Hoechst 33342. Coverslips were mounted with Prolong Gold Antifade Reagent and sealed with nail polish before imaging. Images were captured using an Olympus FV1000 Spectral Confocal Microscope.

Quantification of γ-H2AX: FIJI (ImageJ) software was used to create masks of cells from channel 0 (Hoechst 33342), the masks were then transferred onto channel 1 (anti-γH2AX), and the channel 1 mean gray value within each mask was recorded. At least 200 cells were scored per sample per experiment. The γH2AX mean gray values of individual cells in a representative experiment are shown in extended Fig. E6B.

Senescence-Associated β-Galactosidase Staining: Irradiated (10 Gy) or EV-treated (25μg, 24 hours) MEFs were cultured for additional 5 days in serum-

supplemented media and counterstained with Hoechst 33342 and the Senescence Cells Histochemical Staining Kit (Sigma-Aldrich). The number of nuclei was counted in images captured by the KEYENCE BZ-X700 All-in-One Fluorescence Microscope at a magnification of 20X, with 50% transmitted light, and white balance red-blue-green areas of 1.46, 0.98, and 1.24, respectively. The β-galactosidase positive blue cells were counted under Phase contrast microscope. At least 200 cells were scored per sample per experiment to calculate the percentage of positive senescent cells.

Immunoblotting: Cell pellets were lysed in RIPA buffer (25mM Tris-HCl pH 7.6, 10% Glycerol, 1% NP40, 0.5% sodium deoxycholate, 1x Protease inhibitors (Roche), 150mM Sodium chloride, 50mM Sodium fluoride, 10mM Sodium beta-glycerophosphate, 10mM Sodium orthovandate, 10mM sodium pyrophosphate, 1mM PMSF). Proteins were separated using SDS-PAGE & transferred onto Nitrocellulose membranes (Millipore). Membranes were blocked for 1 hour at room temperature, incubated with anti-Abl (8E9) (1/500) & anti-actin (1/2000) from Sigma Aldrich for 1 hour, washed and incubated with secondary antibody (Anti-mouse: HRP-linked) & developed using ECL reagents (Pierce).

Cell Cycle Analysis: Cells were collected at 24 hours post irradiation or EV treatment by trypsinization, followed by centrifugation at 1400 RPM for 6 min. Cell-pellets were fixed in ice cold 70% ethanol overnight and stained with 40 µg/ml propidium iodide (PI) (Sigma) and 100 µg/ml RNaseA (Sigma) for 30 min at 37°C in the dark. PI staining was analyzed using Sony SH800 FACS sorter and software.

Retrovirus Packaging and Infection: Abl^{WT} & $Abl^{\mu NLS}$ were stably expressed in *Abl- μNLS* MEFs by retroviral infection[29]. BOSC23 cells were transfected with retroviral vector pMSCV expressing Abl^{WT} or $Abl^{\mu NLS}$. Culture media collected at 48 hours after transfection was filtered and added to *Abl-μNLS* MEFs with polybrene (4μg/ml). Infected cells were then selected for resistance to hygromycin (150 μg/ml).

Transfection: Genetran (Biomiga) was used to transfect HEK239T cells with miR-34c-minigene and pCDNA3-AblPPn plasmid DNA[9]. Transfected cells and their media (for EV isolation) were collected 24 hours after transfections.

RNA measurements: The SeraMir Exosome RNA amplification kit (System Biosciences) was used to extract RNA from EV pellets. Total cellular RNA was extracted using TRIzol (Life Technologies). Synthesis of cDNA was carried out using ABI reverse Transcription kit (Life Technologies). For measurements of mature miR-34c, stem-loop primer was used for reverse transcription[30,9]. U6 was used as the reference gene for normalization of miR-34c abundance. GAPDH was used as reference gene for normalization of p21Cip1, Pdgfrb, Pdgfra & Myc abundance. Real-time PCR reactions were carried out using StepOnePlus system. Subtraction of the reference gene CT value from the experimental gene CT value generated the normalized ΔCT. Relative abundance was then calculated as $2^{-\Delta\Delta CT}$, where ΔΔCT values were ΔCT of sample subtracted by ΔCT of vehicle-treated or vector transfected cells. For Primer sequences please refer to the Primer List in Extended Fig. E14B.

Statistical Analysis: The statistical analyses were performed using Graph-Pad Prism 6. For Clonogenic survival & qRT-PCR measurements: the values have been shown as mean ± SD from three independent experiments were analyzed using ONE WAY ANOVA. For ROS & γH2AX measurements the values have been shown as medians with interquartile range from the indicated number of independent experiments (at least 200 cells analyzed per sample per experiment) were analyzed using Kruskal-Wallis test. For each test ns: not significant; *$P \leq 0.05$, **$P \leq 0.01$, *** $P \leq 0.001$, **** $P \leq 0.0001$.

ACKNOWLEDGEMENTS

We thank Chenhui Bian, Neal Shah and Louis Nguyen for excellent technical assistance. We thank Dr. Andrea Ventura, Memorial Sloan Kettering Cancer Centre, New York for the miR34^{WT} and miR34^{TKO} primary MEFs. We thank Dr. Clarke Chen & Dr. Johnny Akers for helping with the Nanoparticle Tracking Analysis.

AUTHOR CONTRIBUTIONS

SR designed and performed the experiments, analyzed the data, and wrote the paper. A.H, J.C, performed experiments and analyzed the data. JYJW conceived of the idea, designed the experiments, analyzed the data and wrote the paper.

References:

1. Mothersill, C. & Seymour, C. Medium from irradiated human epithelial cells but not human fibroblasts reduces the colonogenic survival of unirradiated cells. *Int J Rad Biol*, **71**, 421-427 (1997).
2. Le, M. et al. Exosomes are released by bystander cells exposed to radiation-induced biophoton signals: Reconciling the mechanisms mediating the bystander effect. *Plos One* **12,** (2017).
3. Szatmári, T. C. B. C. et al. Extracellular Vesicles Mediate Radiation-Induced Systemic Bystander Signals in the Bone Marrow and Spleen. *Frontiers in Immunology* **8,** (2017).
4. Burdak-Rothkamm, S., Rothkamm, K. & Prise, K. M. ATM Acts Downstream of ATR in the DNA Damage Response Signaling of Bystander Cells. *Cancer Research* **68,** 7059–7065 (2008).
5. Lakin, N. D. & Jackson, S. P. Regulation of p53 in response to DNA damage . *Oncogene* **18,** 7644–7655 (1999).
6. Baskaran, R. et al. Ataxia telangiectasia mutant protein activates c-Abl tyrosine kinase in response to ionizing radiation. *Nature* **387,** 516–519 (1997).
7. Preyer, M., Shu, C.-W. & Wang, J. Y. J. Delayed activation of Bax by DNA damage in embryonic stem cells with knock-in mutations of the Abl nuclear localization signals. *Cell Death and Differentiation* **14,** 1139–1148 (2007).
8. Wang, J. Y. J. The Capable ABL: What Is Its Biological Function? Molecular and *Cellular Biology* **34,** 1188–1197 (2014).
9. Tu, C.-C. et al. The kinase ABL phosphorylates the microprocessor subunit DGCR8 to stimulate primary microRNA processing in response to DNA damage. *Science Signaling* **8,** (2015).
10. Kaidi, A. & Jackson, S. P. KAT5 tyrosine phosphorylation couples chromatin sensing to ATM signalling. *Nature* **498,** 70–74 (2013).
11. Godlewski, J. *et al.* MicroRNA signatures and molecular subtypes of glioblastoma - MicroRNA signatures and molecular subtypes of glioblastoma - the role of extracellular transfer. *Stem Cell Reports* **8,** 1497–1505 (2017).
12. Valadi, H et al. Exosome-mediated transfer of mRNAs and microRNAs is a novel mechanism of genetic exchange between cells, *Nature Cell Biology*, **9,** 654-659 (2007).
13. Tkach, M. & Théry, C. Communication by Extracellular Vesicles: Where We Are and Where We Need to Go. *Cell* **164,** 1226–1232 (2016).
14. Shurtleff, M., Karfilis, K. V., Temoche-Diaz, M., Ri, S. & Schekman, R. Y-box protein 1 is required to sort microRNAs into exosomes in cells and in a cell-free reaction. *eLife* (2016). doi:10.1101/040238
15. Thery, C. et al. Isolation and characterization of exosomes from cell culture supernatants and biological fluids. *Current Protocols in Cell Biology*, 3.22.1-3.22.29 (2006).
16. Shelke, G. V., Lässer, C., Gho, Y. S. & Lötvall, J. Importance of exosome depletion protocols to eliminate functional and RNA-containing extracellular vesicles from fetal bovine serum. *Journal of Extracellular Vesicles* **3,** 24783 (2014).
17. Havaki, S. et al. The role of oxidative DNA damage in radiation induced bystander effect. *Cancer Letters* **356,**43–51 (2015).
18. Al-Mayah, A. *et al.* The non-targeted effects of radiation are perpetuated by exosomes. *Mutation Research/Fundamental and Molecular Mechanisms of Mutagenesis* **772,** 38–45 (2015).
19. Morgan, W. F. & Sowa, M. B. Non-targeted effects induced by ionizing radiation: Mechanisms and potential impact on radiation induced health effects. *Cancer Letters* **356,** 17–21 (2015).
20. Polo, S. E. & Jackson, S. P. Dynamics of DNA damage response proteins at DNA breaks: a focus on protein modifications. *Genes & Development* **25,** 409–433 (2011).
21. Pires, E., Sung, P. & Wiese, C. Role of RAD51AP1 in homologous recombination DNA repair and carcinogenesis. *DNA Repair* **59,** 76–81 (2017).

22. Sridevi, P., Nhiayi, M. K. & Wang, J. Y. J. Genetic disruption of Abl nuclear import reduces renal apoptosis in a mouse model of cisplatin-induced nephrotoxicity. *Cell Death and Differentiation* **20,** 953–962 (2013).
23. He, L., He, X. & Lim, L. P. A microRNA component of the p53 tumour suppressor network. *Nature* **447,** 1130-1134 (2007).
24. Concepcion, C. P. et al. Intact p53-Dependent Responses in miR-34–Deficient Mice. *PLoS Genetics* **8,** (2012).
25. Garofalo, M. et al. MiR-34a/c-dependent PDGFR-α/β downregulation inhibits tumorigenesis and enhances TRAIL-induced apoptosis in lung cancer. *Plos One* **8,** (2013).
26. Cannell, I. G. et al. p38 MAPK/MK2-mediated induction of miR-34c following DNA damage prevents Myc-dependent DNA replication. *Proceedings of the National Academy of Sciences* **107,** 5375–5380 (2010).
27. Akers, J. C. et al. Comparative Analysis of Technologies for Quantifying Extracellular Vesicles (EVs) in Clinical Cerebrospinal Fluids (CSF). *Plos One* **11,** (2016).
28. Mineo, M. et al. Exosomes released by K562 chronic myeloid leukemia cells promote angiogenesis in a src-dependent fashion. Angiogenesis 15, 33–45 (2011).
29. Pear, W. S., Scott, M. L. & Nolan, G. P. Generation of High-Titer, Helper-Free Retroviruses by Transient Transfection. *Gene Therapy Protocols* **41–58** (1994). doi:10.1385/0-89603-484-4:41
30. Chen, C. et al. Real-time quantification of microRNAs by stem-loop RT-PCR. *Nucleic Acids Research* **33,** e179 (2005).

Figure 1.

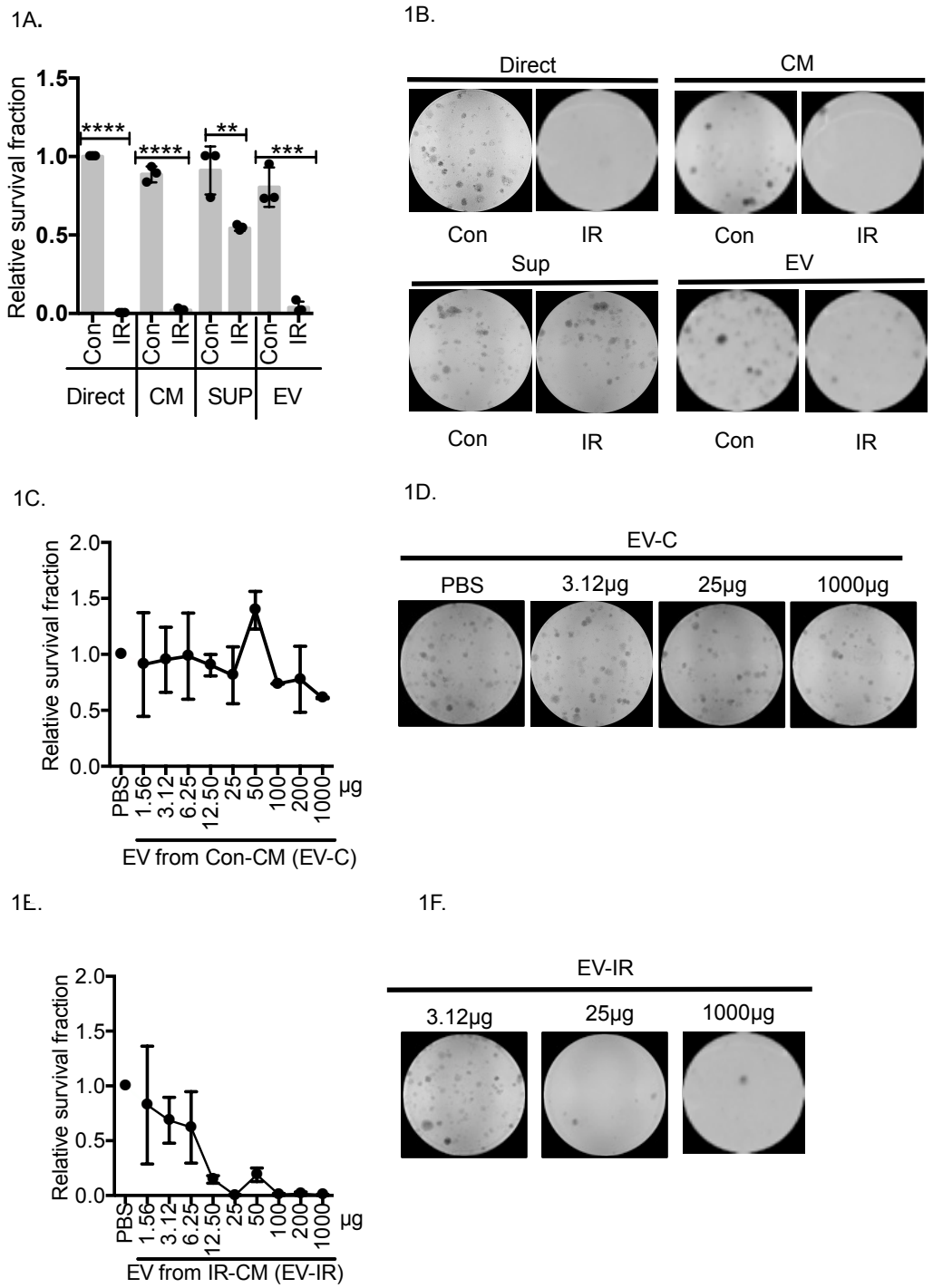

Figure 1. Extracellular Vesicles from Irradiated Cells (EV-IR) Inhibited Colony Formation

(A) Clonogenic survival of MEFs at 15 days after the following treatments: non-irradiated (Direct, Con), 10Gy irradiated (Direct, IR), treated for 24 hours with CM

(conditioned media), Sup (supernatant fraction of CM), or EV (extracellular vesicle pellet fraction of CM, 25μg each) from non-irradiated (Con) or 10Gy irradiated (IR) MEFs. CM was collected 24 hours after radiation. Sup & EV were isolated from the CM (Fig. E1). The survival fraction (number of colonies/number of cells seeded) of non-irradiated MEFs was set to 1. Values shown are mean ± SD from three independent experiments. $^{**}P<0.01$, $^{***}P<0.0001$, $^{****}P< 0.0001$, One Way ANOVA.

(B) Representative images of colonies in the indicated samples as in (A).

(C) Clonogenic survival of MEFs at 15 days after treatments for 24 hours with PBS or the indicated concentrations of EV-C isolated from CM of non-irradiated MEFs. The survival fraction of PBS treated sample was set to 1. Values shown are mean ± SD from two independent experiments.

(D) Representative images of colonies in the indicated samples as in (C).

(E) Clonogenic survival of MEFs at 15 days after treatments for 24 hours with PBS or the indicated concentrations of EV-IR isolated from CM of irradiated MEFs. The survival fraction of PBS treated sample was set to 1. Values shown are mean ± SD from two independent experiments.

(F) Representative images of colonies in the indicated samples as in (E).

Figure 2.

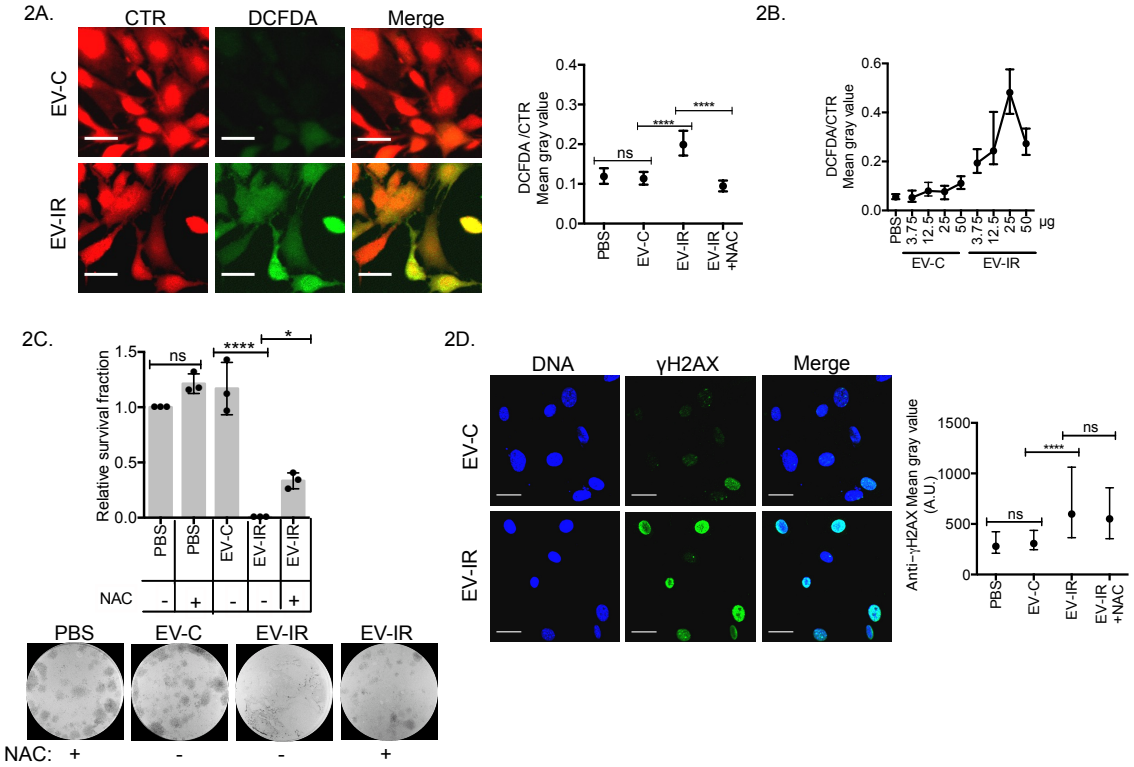

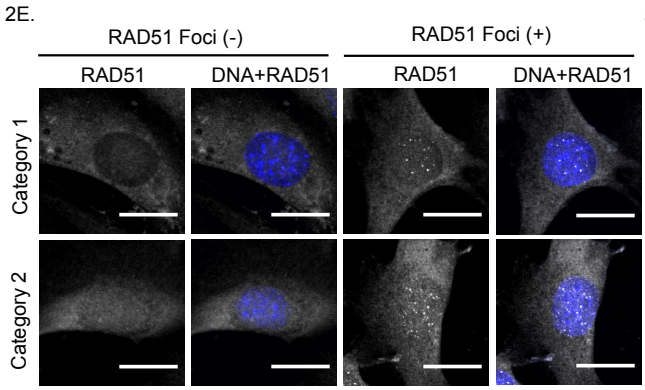

2F.

Treatment	EV-C	EV-IR
% RAD51 Foci (+) nuclei	89/423 21%	171/355 48%
(Category 1)	12/283 4%	40/212 19%
(Category 2)	77/140 55%	131/143 92%

Figure 2. EV-IR Induced Reactive Oxygen Species (ROS) & Bystander DNA Damage

(A) EV-IR but not EV-C increased ROS: live cells were stained with Cell-tracker red (CTR) and DCFDA (green) at 24 hours after addition of EV-C, EV-IR or EV-IR+NAC (3.5µg each of EV, 5mm NAC) (Scale bar: 35µm). Ratio of DCFDA/CTR staining was calculated as described in Methods. Values shown are medians with interquartile ranges from three independent experiments with at least 200 cells analyzed per sample per experiment. ns, not significant; ****$P \leq 0.0001$, Kruskal-Wallis test. The DCFDA/CTR ratios of individual cells are shown in Fig. E6A.

(B) EV-IR dose-dependency in inducing ROS: responder MEFs were treated with the indicated concentrations of EV-C or EV-IR for 24 hours and the ROS measured as in (A). Values shown are the medians and interquartile ranges of ratios from two independent experiments with at least 200 cells analyzed per sample per experiment.

(C) NAC reduced the colony-inhibitory activity of EV-IR: Clonogenic survival of responder MEFs at 15 days after treatment for 24 hours with 25μg each of EV-C, EV-IR, or EV-IR+NAC (5mM). Relative survival fractions shown are mean ± SD from three independent experiments. ns, not significant; * $P \leq 0.05$, **** $P \leq 0.0001$, One Way ANOVA.

(D) EV-IR but not EV-C increased γH2AX: responder MEFs were fixed at 24 hours after addition of 3.5μg each of EV-C, EV-IR or EV-IR+NAC (5mM) and stained with anti-γH2AX (Green) & Hoechst 33342 (DNA; blue) (Scale bar: 35μm) and the γH2AX levels quantified as described in Methods. Values shown are medians with interquartile ranges from three independent experiments with at least 200 cells analyzed per experiment. ns, not significant; **** $P \leq 0.0001$, Kruskal-Wallis test. The mean gray values of γH2AX in individual cells in are shown in Fig. E6B.

(E) Images of RAD51 foci: Responder cells were fixed and stained with anti-RAD51 (Green) & Hoechst 33342 (DNA; blue) at 24 hours after addition of EV-C or EV-IR (25μg each) (Scale bar: 25μm). Representative images of RAD51 staining category-1 (darker nuclei) or 2 (brighter nuclei) with or without foci are shown.

(F) EV-IR but not EV-C increased RAD51 foci: Summary of RAD51 foci-positive nuclei in each indicated samples with breakdowns into categories. Representative images of multiple cells in each sample are shown in Fig. E7.

Figure 3.

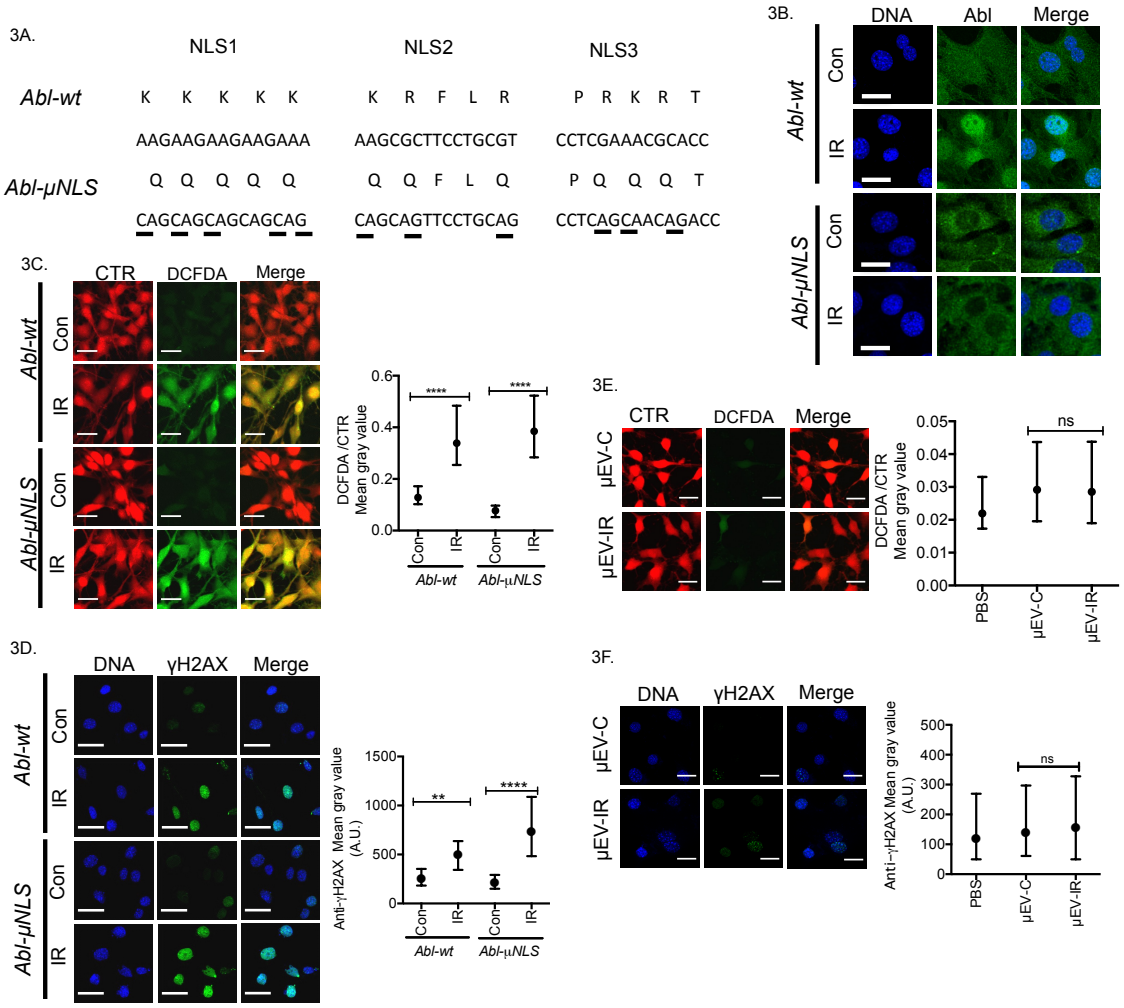

Figure 3. Extracellular Vesicles from Irradiated *Abl-μNLS* MEFs (μEV-IR) Failed to Induce Bystander Effects.

(A) Substitution mutations of the three Abl nuclear localization signals (NLS) in the *Abl-μNLS* allele[7].

(B) Representative immunofluorescence images of Abl (green) and DNA (blue) staining in the indicated MEFs: Con, no irradiation; IR: 3 hours after 10Gy (Scale bar: 30μm).

(C) Direct irradiation Induced ROS in *Abl–μNLS* MEFs: the indicated cells were stained with Cell-tracker red (CTR) and DCFDA (green) at 24 hours after no irradiation (Con) or 10Gy of IR (Scale bar: 35μm). Ratio of DCFDA/CTR staining was determined as described in Methods. Values shown are the medians with interquartile ranges from two independent experiments with at least 200 cells analyzed per sample per experiment. **** $P \leq 0.0001$, Kruskal-Wallis test.

(D) Direct irradiation increased γH2AX in *Abl-μNLS* MEFs: the indicated cells were fixed and stained with anti-γH2AX (green) and Hoechst 33342 (DNA; blue) at 24 hours after no irradiation or 10Gy IR (Scale bar: 35μm). The γH2AX levels

were determined as described in Methods. Values shown are medians with interquartile ranges from two independent experiments with at least 200 cells analyzed per experiment. ** $P \leq 0.01$, **** $P \leq 0.0001$, Kruskal-Wallis test.

(E) μEV-IR did not increase ROS: responder MEFs (*Abl-wt*) stained with the indicated dyes at 24 hours after treatment with μEV-C & μEV-IR (3.5μg each) isolated from CM of non-irradiated or irradiated (10Gy IR) *Abl–μNLS* MEFs (Scale bar: 35μm). Values of DCFDA/CTR ratios shown are the medians with interquartile ranges from three independent experiments with at least 200 cells analyzed per sample per experiment. ns: not significant, Kruskal-Wallis test

(F) μEV-IR did not increase γH2AX: responder MEFs (*Abl-wt*) were fixed and stained at 24 hours after treatment with μEV-C & μEV-IR (3.5μg each) (Scale bar: 35μm). Values shown are medians with interquartile ranges from three independent experiments with at least 200 cells analyzed per experiment. ns, not significant, Kruskal-Wallis test.

Figure 4.

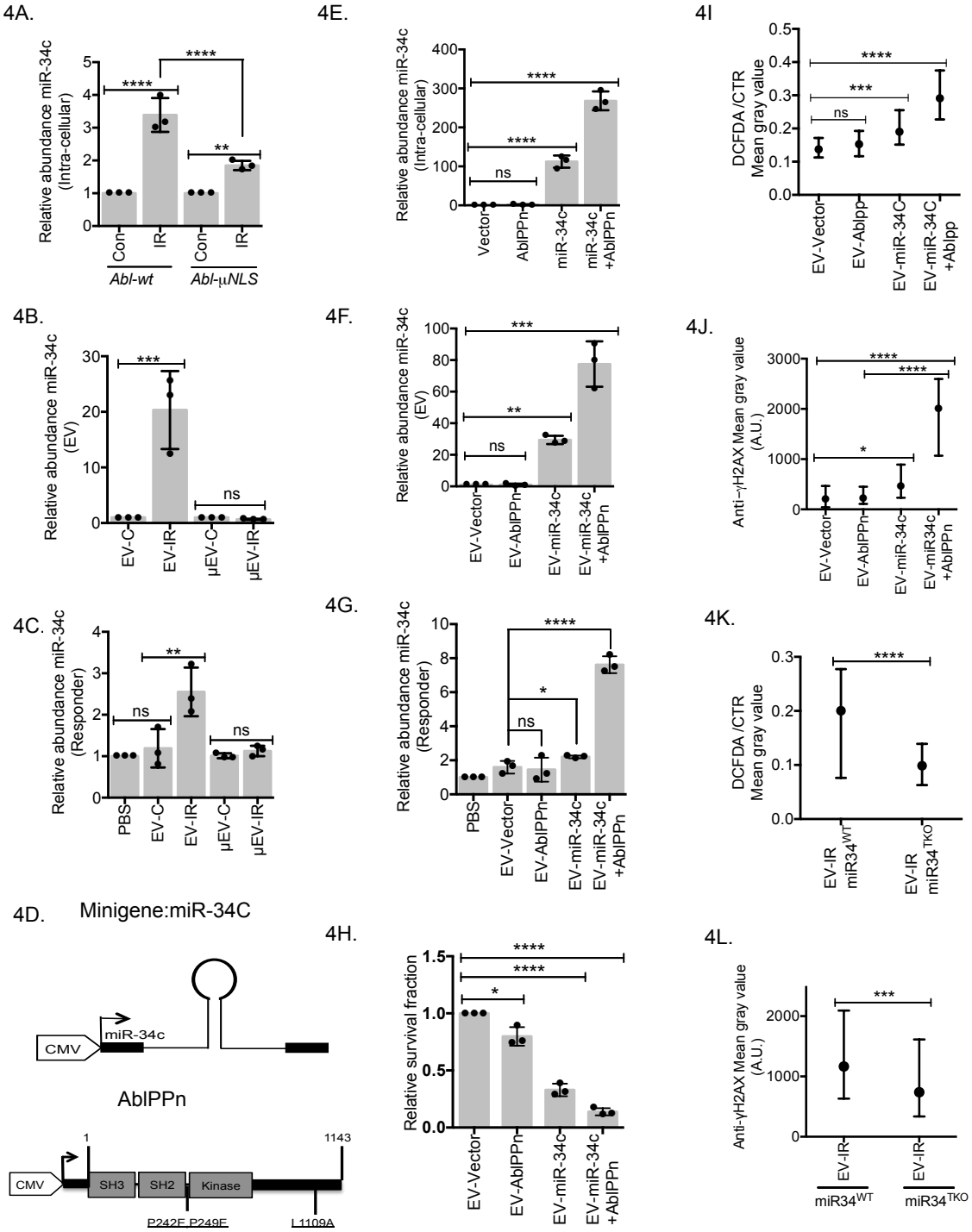

Figure 4: miR-34c-containing EV Induced Bystander Effects of Radiation
(A) Irradiation increased intra-cellular levels of miR-34c: *Abl-wt* & *Abl-μNLS* MEFs were irradiated at 10Gy, RNA was collected after 24 hours, and miR-34c

measured as described in Methods. Abundance of miR-34c normalized to that of U6 in non-irradiated (Con) MEFs was set to 1. Values shown are relative miR-34c abundance (mean ± SD) from three independent experiments. ** $P \leq 0.01$, ****$P \leq 0.0001$, ONE WAY ANOVA.

(B) Irradiation increased miR-34c levels in EV-IR but not in μEV-IR: Relative abundance of miR-34c in EV-C and EV-IR or μEV-C and μEV-IR isolated from CM of non-irradiated or irradiated (10Gy) *Abl-wt* or *Abl-μNLS* MEFs, respectively. Values shown are relative abundance (mean ± SD) with the normalized miR-34c level in EV-C or μEV-C set to 1 from three independent experiments. ns, not significant; ***$P \leq 0.001$, ONE WAY ANOVA.

(C) EV-IR raised miR-34c levels in responder MEFs: non-irradiated MEFs (*Abl-wt*) treated with the indicated EV (25μg) were harvested at 24 hours and miR-34c in total RNA measured as described in Methods. The normalized miR-34c abundance in PBS-treated cells was set to 1. Values shown are relative abundance (mean ± SD) from three independent experiments. ns: not significant; **$P \leq 0.01$, ONE WAY ANOVA.

(D) Schematic diagrams of the miR-34c minigene and the AblPPn expression construct[9].

(E, F) Co-transfection of miR-34c-minigene with AblPPn raised intra-cellular (E) and EV (F) miR-34c levels: HEK293T cells transfected with vector, AblPPn, miR-34c-minigene or miR-34c-minigene+AblPPn were collected at 24 hours post transfection and the media from the transfected cells were harvested for EV collection. Normalized miR-34c abundance in vector-transfected cells (E), or in EV isolated from vector-transfected cells (F), was set to 1. Values shown are mean ± SD from three independent experiments. ns: not significant; **$P \leq 0.01$, ***$P \leq 0.001$, ****$P \leq 0.0001$, One Way ANOVA.

(G) Treatment with EV-miR-34c and EV-miR-34c+AblPPn raised miR-34c levels in responder MEFs: non-irradiated MEFs (*Abl-wt*) were treated with PBS or the indicated EV preparations (25μg) for 24 hours. Normalized miR-34c abundance in PBS-treated MEFs was set to 1. Values shown are mean ± SD from three independent experiments. ns: not significant; *$P \leq 0.05$, ****$P \leq 0.0001$, ONE WAY ANOVA.

(H) miR-34c-containing EV inhibited colony formation: clonogenic survival fraction of responder MEFs at 15 days after treatments for 24 hours with the indicated EV (25μg) from the transfected HEK293T cells. Survival fraction of EV-vector treated sample was set to 1. Values shown are relative survival fraction (mean ± SD) from three independent experiments. *$P \leq 0.05$, ****$P \leq 0.0001$, ONE WAY ANOVA.

(I) miR-34c-containing EV induced ROS: DCFDA/CTR ratios in responder MEFs at 24 hours after treatment with the indicated EV (25μg) from the transfected HEK239T cells. Values shown are medians with interquartile ranges from three independent experiments with at least 200 cells analyzed per sample per experiment. ns: not significant; ***$P \leq 0.001$, ****$P \leq 0.0001$, Kruskal Wallis test. Representative images and the ratios of individual cells from one experiment are shown in Fig. E13C, D.

(J.) miR-34c-containing EV increased γH2AX: Levels of γH2AX in responder MEFs at 24 hours after treatment with the indicated EV (25μg) from the transfected HEK239T cells. Values shown are medians with interquartile ranges from two independent experiments with at least 200 cells analyzed per experiment. *$P \leq 0.05$,****$P \leq 0.0001$, Kruskal-Wallis test. Representative images and the mean gray values of individual cells from one experiment are shown in Fig. E13E, F.

(K) EV-IR from miR34^{TKO} MEFs failed to induce ROS: DCFDA/CTR ratios in responder MEFs (*Abl-wt*) treated with PBS or the indicated EV-IR (25μg each) isolated from irradiated miR34^{WT} or miR34^{TKO} MEFs. Values shown are medians with interquartile ranges from two independent experiments with at least 200 cells analyzed per experiment. ****$P \leq 0.0001$, Kruskal-Wallis test. Representative images and the ratios of individual cells from one experiment are shown in Fig. E13G, H.

(L) EV-IR from miR34^{TKO} cells increased γH2AX with reduced activity: Levels of γH2AX in responder MEFs (*Abl-wt*) treated with PBS or the indicated EV-IR (25μg each) isolated from irradiated miR34^{WT} or miR34^{TKO} MEFs. Values shown are medians with interquartile ranges from two independent experiments with at least 200 cells analyzed per experiment. ***$P \leq 0.001$, Kruskal-Wallis test. Representative images and the mean gray values of individual cells in each experimental sample are shown in extended Fig. E13I, J.

Extended Figure 1.

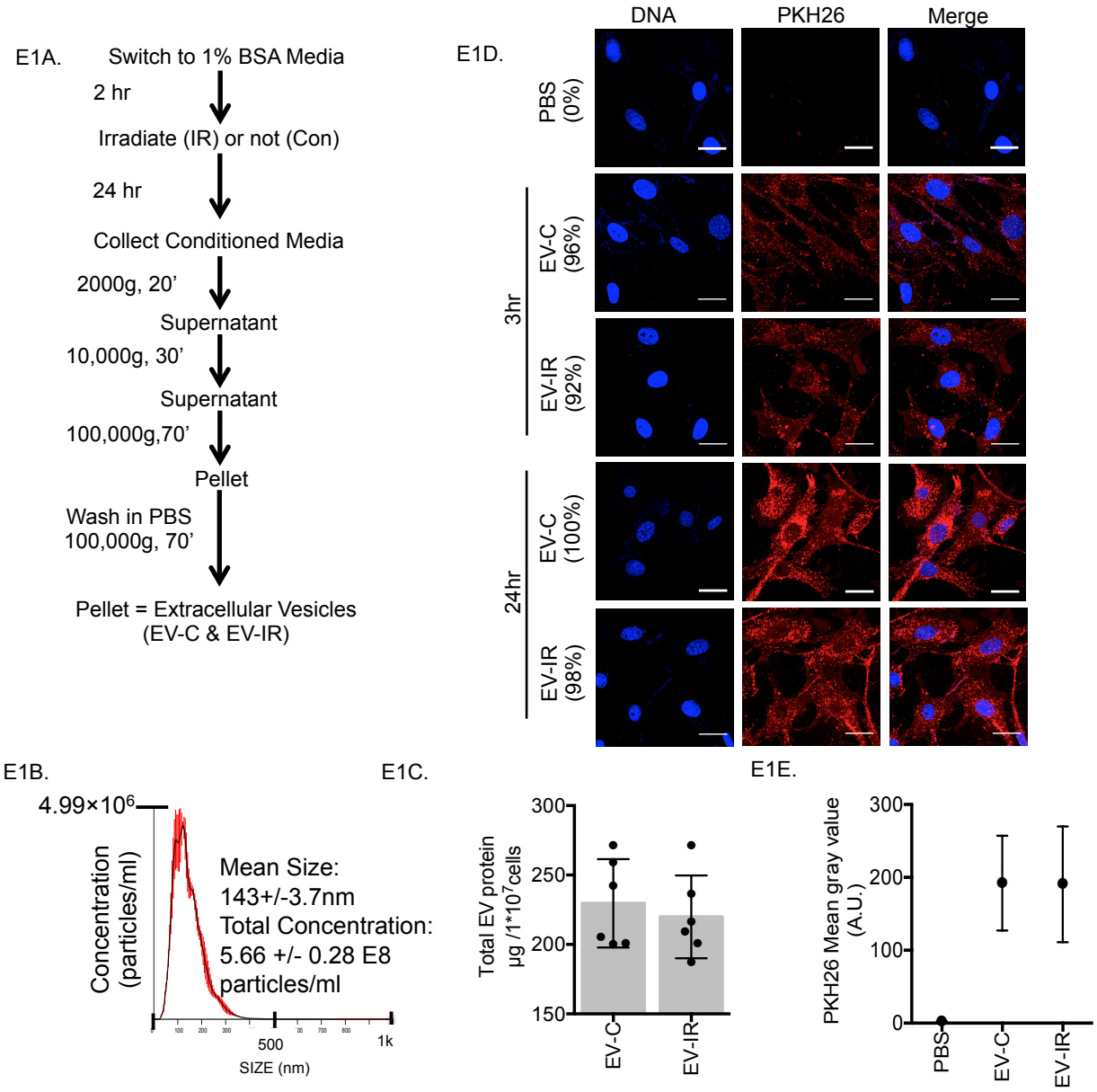

Extended Figure 1. Extracellular vesicle (EV) isolation, quantification and uptake

(A). Flow-chart summarizing the EV isolation protocol using ultracentrifugation method from FBS free media with 1% BSA conditioned by non-irradiated (Con) or irradiated (IR 10Gy) mouse embryo fibroblasts for 24 hours.

(B). Nanoparticle tracking analysis of a typical EV preparation (EV-C or EV-IR). Nanoparticle tracking analysis uses the diffraction measurement of Brownian

motion of the EV particles, which is then captured by camera over a series of frames to determine the particle size & concentration[27]. Graph displays the total concentration and mean size of the particles.

(C). Total protein in EV-C or EV-IR from media conditioned by the indicated number of *Abl-wt* MEFs (Non-irradiated or irradiated at 10Gy for 24 hours). Values shown are mean ± SD from six independent EV preparations.

(D). Uptake of PKH26-labeled EV-C (25μg) and EV-IR (25μg) by naïve, non-irradiated MEFs detected by fluorescence microscopy at 3 & 24 hours after EV addition. Representative images (Scale bar: 35μm) with the percentage of cells stained positive for PKH26 indicated. Note that PKH26 dye was added to the PBS sample but the signal was too dilute to be visualized.

(E). Quantification of PKH26 mean gray values in MEFs treated with PKH26-PBS, PKH26-EV-C or PKH26-EV-IR (25μg). The mean and standard deviation of PKH26 pixel intensities from at least 200 cells are shown.

Extended Figure 2.

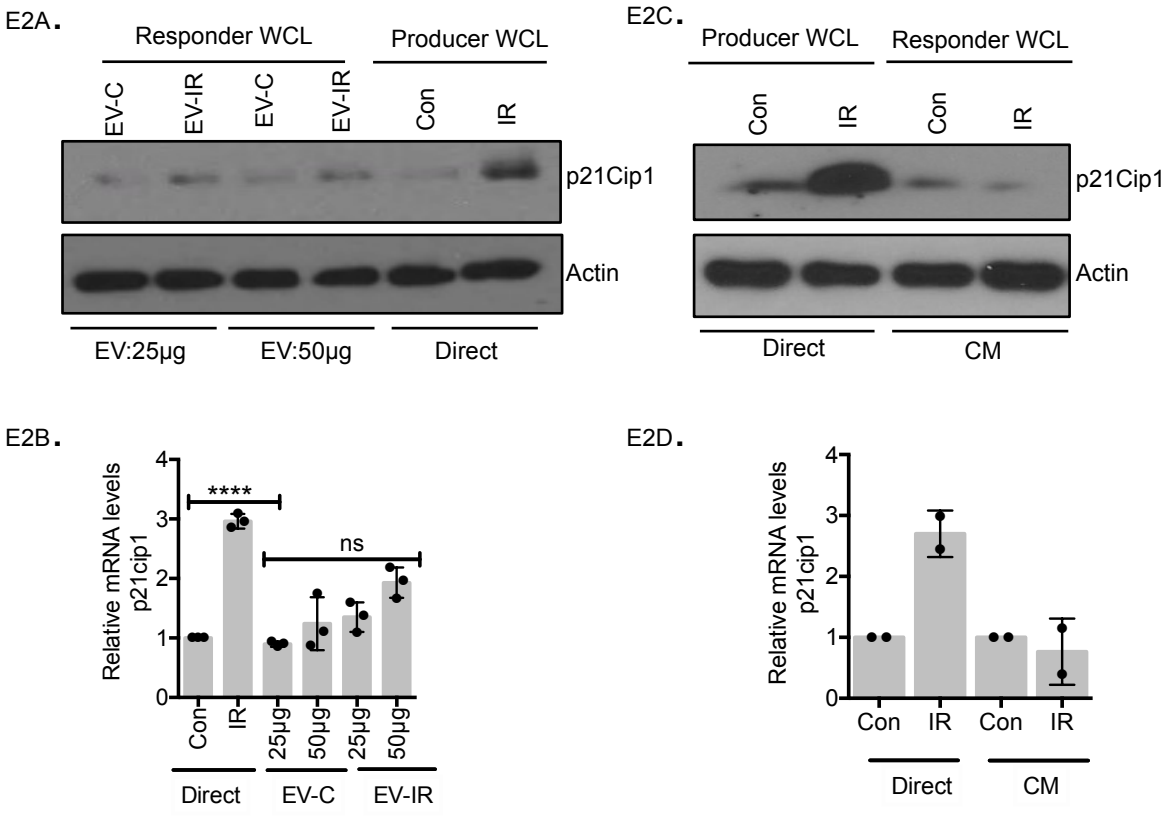

Extended Figure 2. Direct irradiation but not EV-IR stimulated p21 expression

(A). Western blotting with anti-p21Cip1 of whole cell lysates (WCL) from MEFs after 24 hours of treatment with indicated EV samples at two different concentrations (25μg & 50μg) or direct irradiation (10Gy).

(B). Relative abundance of p21Cip1 RNA in MEFs after 24 hours of treatment with indicated EV samples at two different concentrations (25μg & 50μg) or direct irradiation (10Gy). Normalized p21Cip1 abundance in non-irradiated MEFs was set to 1. Data presented as (mean ± SD) from three independent experiments. ns: not significant, **** $P < 0.0001$, ONE WAY ANOVA.

(C). Western blotting with anti-p21Cip1 of whole cell lysates (WCL) from MEFs after 24 hours of treatment with indicated CM samples or direct irradiation.

(D). Relative abundance of p21Cip1 RNA in MEFs after 24 hours of treatment with indicated CM samples or direction irradiation. Normalized p21Cip1 abundance in non-irradiated MEFs was set to 1. Data presented as (mean ± SD) from two independent experiments.

Extended Figure 3.

E3A.

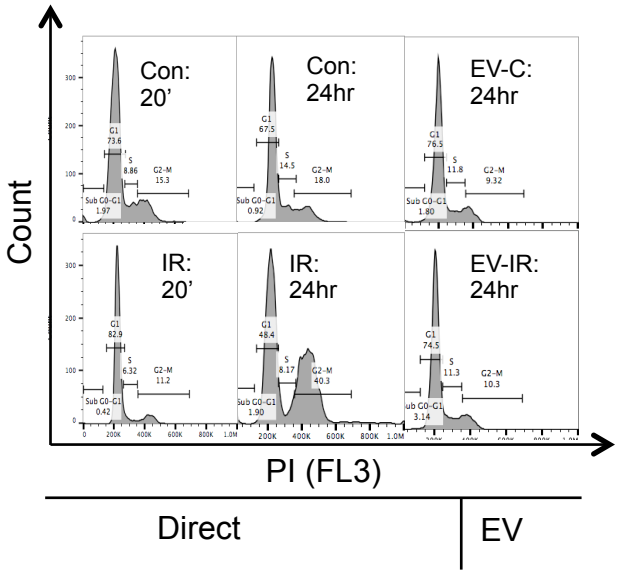

E3B.

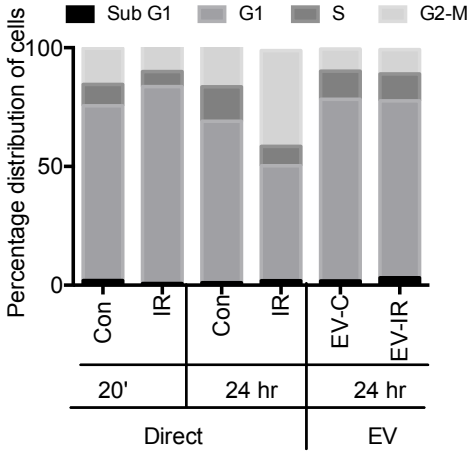

Extended Figure 3. Direct irradiation but not EV-IR caused cell-cycle arrest (A). FACS analysis of DNA content: MEFs were collected at the indicated times after 10Gy irradiation (IR) or not (Con), or at 24 hours after treatment with EV-C or EV-IR (25μg). Representative FACS line graphs with cell cycle distribution determined by the software FlowJo are shown.

(B). Stacked bar graph summarizing the cell cycle distribution of MEF populations after the indicated treatments. Data collected from one independent experiment.

Extended Figure 4.

E4A.

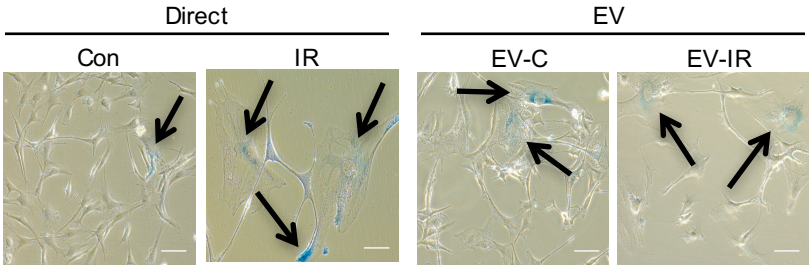

E4B.

β-gal Assay : Senescence indicator Day 10 (% β-gal positive cells)	
Direct	EV
Con: 3.2%±0.3%	EV-C: 4.5%±0.2%
IR: 94%±0.5%	EV-IR: 6.4%±0.3%

Extended Figure 4. Direct irradiation but not EV-IR induced senescence

(A). Directly irradiated or EV-treated (25μg, 24 hours) MEFs were cultured for 10 days and stained for β-galactosidase. Representative images with β-galactosidase-positive (blue) cells are marked with arrows (Scale bar: 30μm).

(B). Quantification of at least 200 senescent cells counted per sample per experiment. Values shown in (B) are (mean ± SD) from two independent experiments.

Extended Figure 5

E5A.

Samples	Relative survival fractions	Relative ROS levels
PBS	1	1
EV-C	0.83	1.3
EV-IR	0.02	3.2
Proteinase-K treated EV-IR	0.05	2.6
RNase-A treated EV-IR	0.04	2.9

Extended Figure 5. Protease and RNase Treatment had no effect on the BE-inducing activity of EV-IR

(A). Relative survival fraction & relative ROS levels in responder MEFs treated with indicated treatments & collected after 24 hours. Isolated EV were incubated with proteinase K (0.05mg/ml) for 10 min at 60°C or with RNaseA (0.5mg/ml) for 20 min at 37°C to degrade unprotected protein & RNA. Data collected from one independent experiment for each relative survival fractions & ROS levels.

Extended Figure 6

E6A.

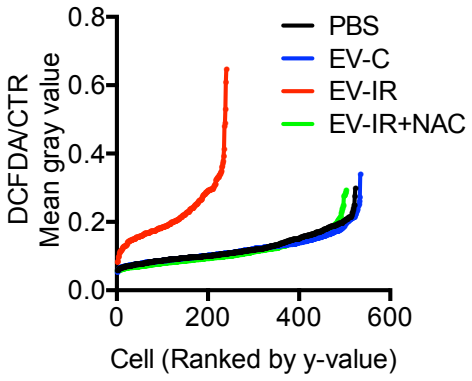

E6B.

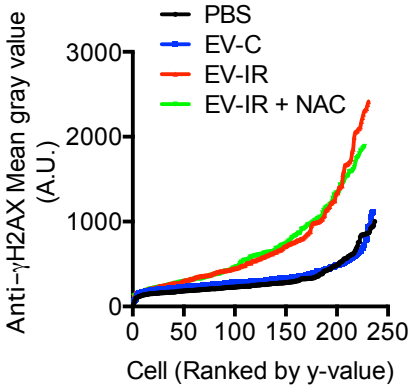

Extended Figure 6. Mean gray values of DCFDA/CTR and γH2AX in individual cells from representative experiments

(A). The ratio of DCFDA/CTR mean gray values for individual cells from one of the three experiments shown in Fig. 2A.

(B). The γ-H2AX mean gray values of individual cells from one of the three experiments shown in Fig. 2D.

Extended Figure 7

E7A.

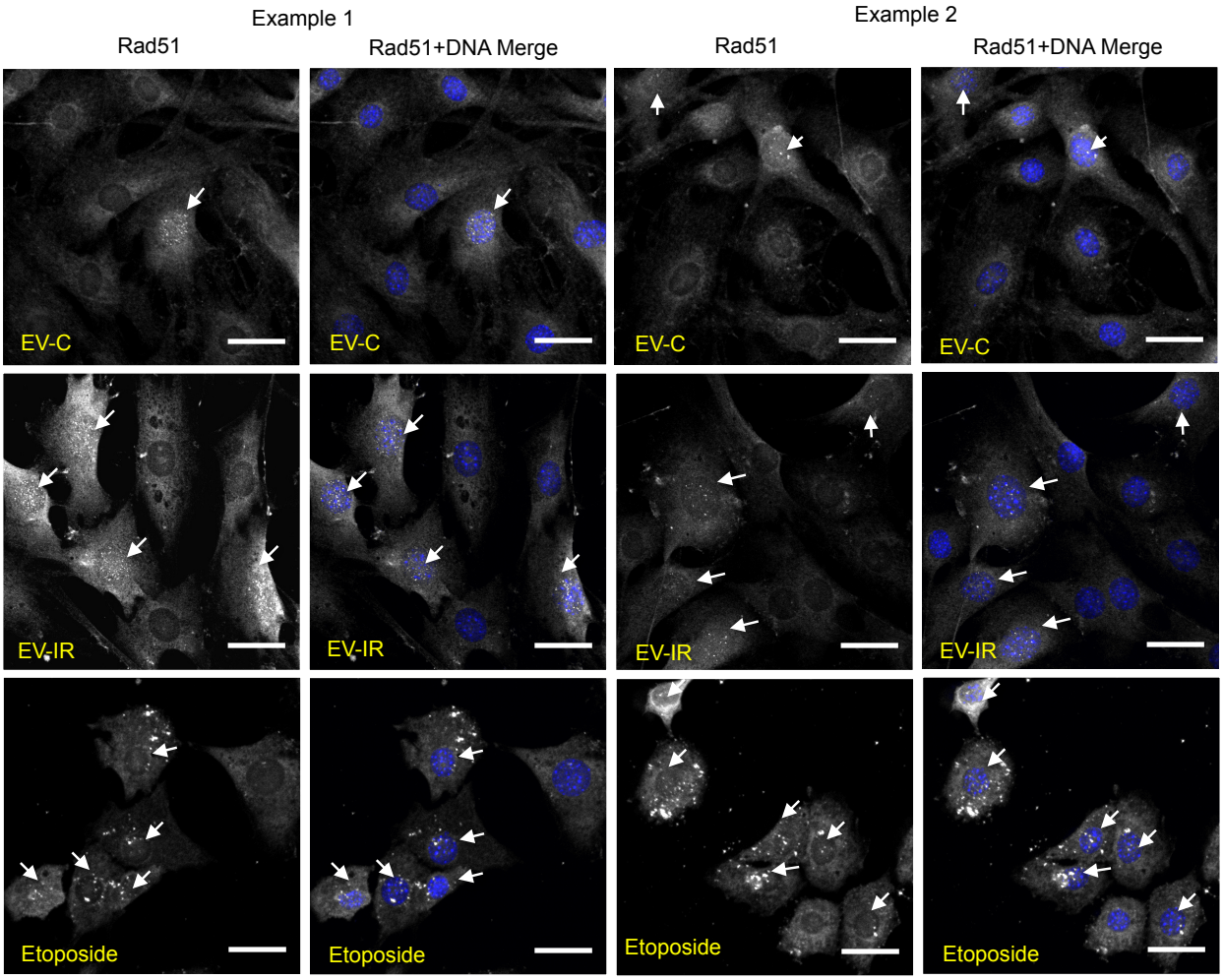

E7B.

Treatment	EV-C	EV-IR
# of Images Counted	26	31
Total Scored Nuclei	423	355
Category 1	283	212
Category 2	140	143

Extended Figure 7. Representative images of RAD51 foci

(A). MEFs treated with EV-C or EV-IR (25μg each) or with Etoposide (20μM) for 24 hours were fixed and stained with anti-RAD51 and Hoechst. Two

representative images are shown for each treatment. The white arrows point to nuclei with RAD51 foci.

(B). Summary of total nuclei scored for the data shown in Fig. 2F.

Extended Figure 8

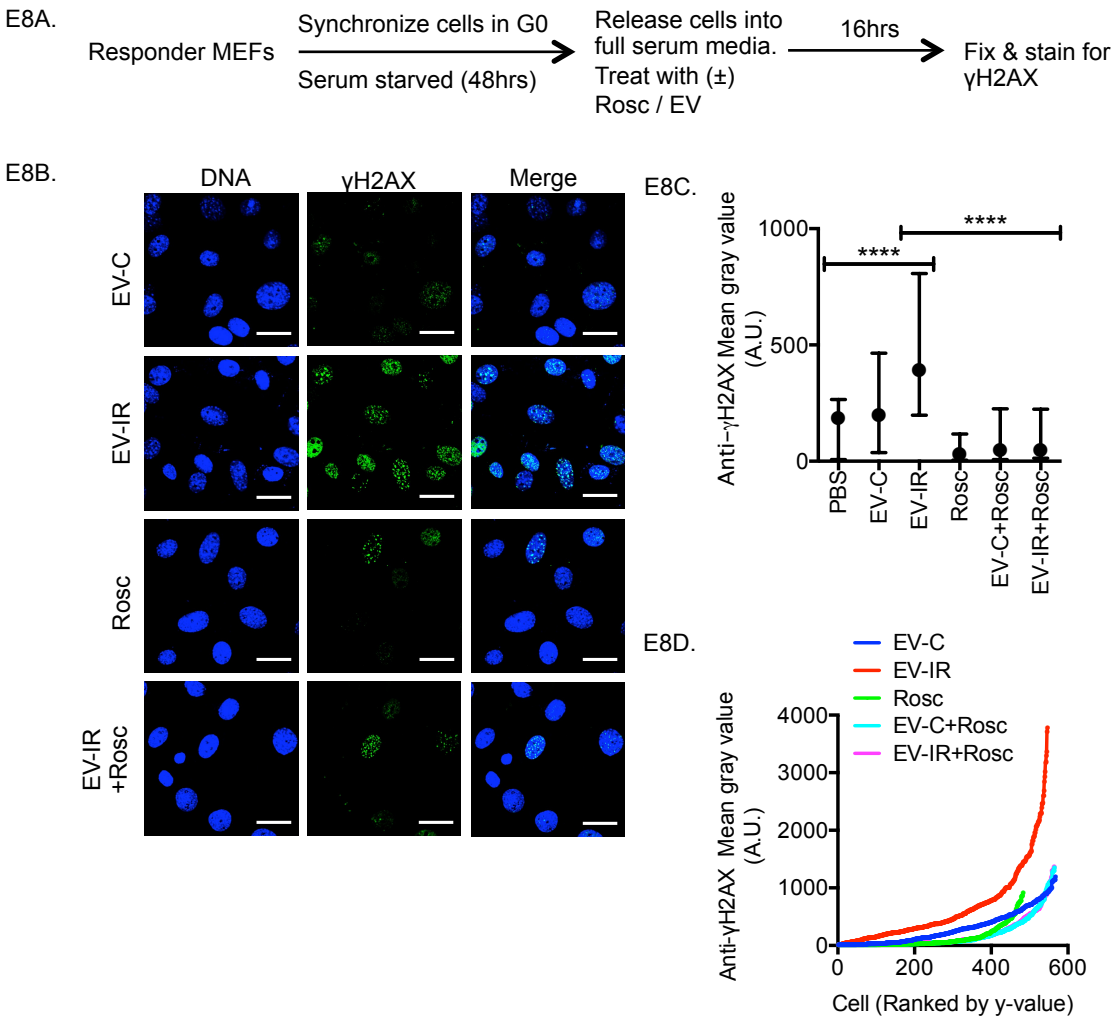

Extended Figure 8. Roscovitine blocked EV-IR-induced increase in γH2AX

(A). Flow-chart of experimental protocol. Responder MEFs were synchronized by serum starvation and then released by serum addition and the indicated treatments. Cells were fixed and stained with anti-gH2AX at 16 hours after addition of serum, Roscovitine and/or EVs.

(B). Representative images of γH2AX staining: responder MEFs were serum starved for 48 hours and then released into full serum media ± Roscovitine (10μM) and treated with EV-C or EV-IR (25μg each) for 16 hours before fixation

and staining with anti-γH2AX (green) and Hoechst 33342 dye (DNA: blue) (Scale bar: 35μm).

(C). The γH2AX mean gray values of the indicated treatments are shown as median with interquartile range with at least 500 cells analyzed per sample. ****$P \leq 0.0001$. Kruskal-Wallis test.

(D). The γ-H2AX mean gray values of individual cells from each of the indicated treatments.

Extended Fig 9.

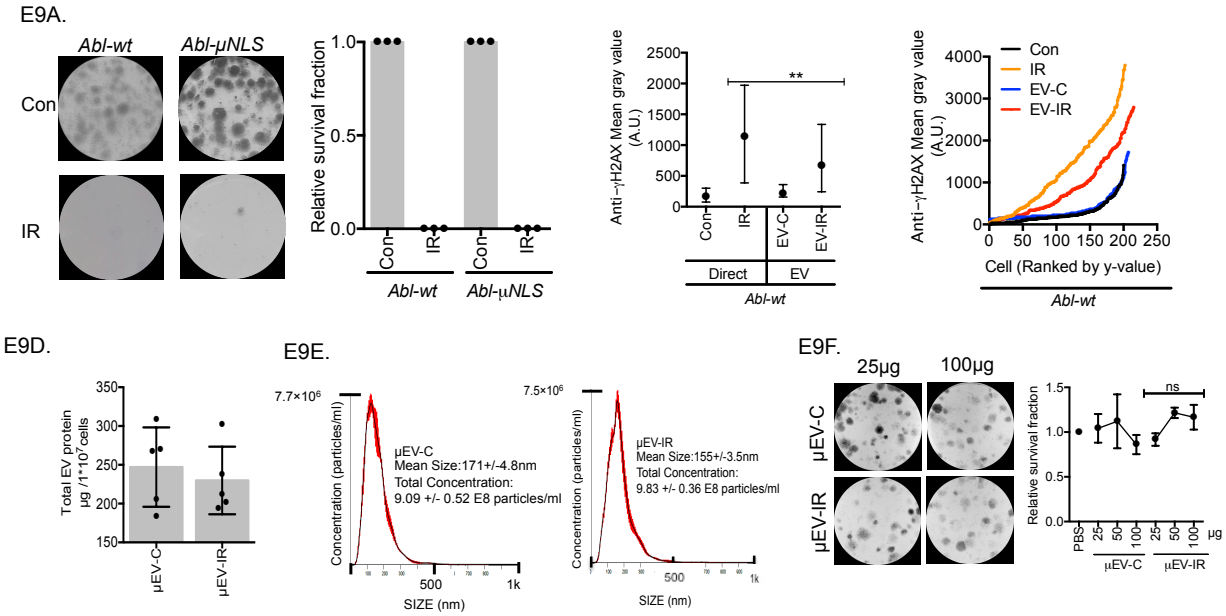

Extended Figure 9. Additional information on *Abl-μNLS* MEFs, μEV-C and μEV-IR

(A). Representative images & quantification for clonogenic survival fraction in directly irradiated (10 Gy) *Abl-wt* & *Abl-μNLS* MEFs. Values shown are relative survival fractions (mean ± SD) from three independent experiments.

(B). The γH2AX mean gray values in the indicated samples are shown as median with interquartile range from one independent experiment with at least 200 cells analyzed per sample. ***P*≤ 0.01. Kruskal-Wallis test.

(C). The γ-H2AX mean gray values of individual cells in the experiment for Fig. E9B.

(D). Total protein in μEV-C & μEV-IR from media conditioned by the indicated number of *Abl-μNLS* MEFs, either non-irradiated or 10Gy irradiated. Values shown are mean ± SD from 5 independent preparations of μEV-C or μEV-IR.

(E). Nanoparticle tracking analysis to determine the size distribution and concentration of particles in a typical μEV-C & μEV-IR preparation.

(F.) Representative images & quantification for clonogenic survival fraction in responder MEFs treated with PBS or 25, 50, and 100μg each of μEV-C or μEV-

IR and survival fraction determined as described in Methods. Values shown are relative survival fraction (mean ± SD) from three independent experiments. ns: not significant, ONE WAY ANOVA.

Extended Fig 10.

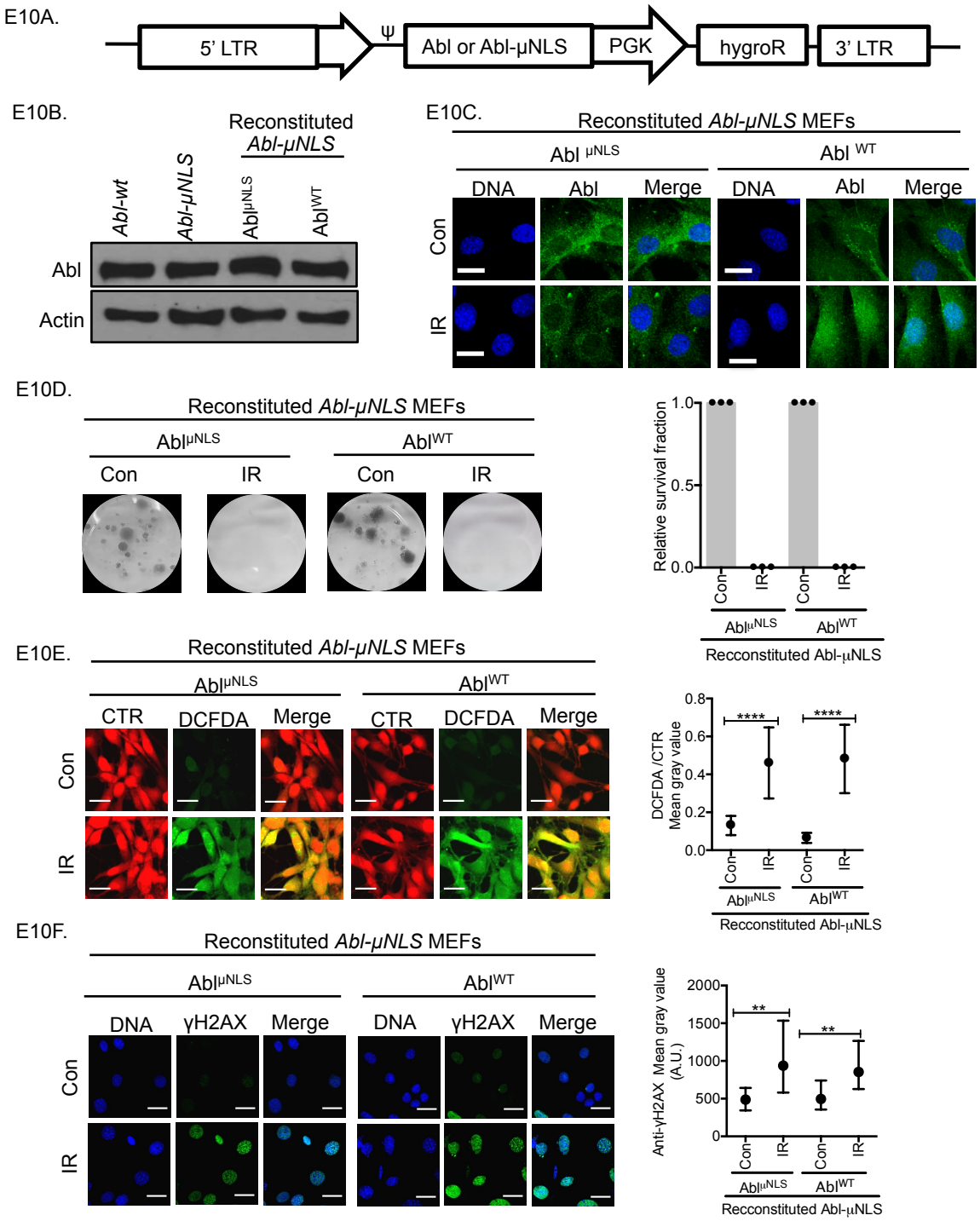

Extended Figure 10. Re-expression of Abl$^{\mu NLS}$ & Abl^{WT} in *Abl-μNLS* MEFs

(A). Retroviral vector used to express Abl$^{\mu NLS}$ & Abl^{WT} in *Abl-μNLS* MEFs.

(B). Immunoblotting of Abl in whole cell lysates from the indicated MEFs.

(C). Representative images of Abl localization at 3 hours after irradiation (10Gy) in the indicated MEFs. DNA: blue, Abl: green (Scale bar: 35μm).

(D). Representative images & quantification of clonogenic survival fraction in directly irradiated MEFs after irradiation (10Gy). Values shown are relative survival fraction (mean ± SD) from three independent experiments.

(E). Representative images & quantification of ROS: the indicated live cells were stained with Cell-tracker red (CTR), and DCFDA (green) at 24 hours post irradiation (10 Gy) (Scale bar: 50μm). Mean gray value ratio of DCFDA/CTR was calculated for each cell. Values shown are the median with interquartile range from two independent experiments with at least 200 cells analyzed per sample per experiment. **** $P \leq 0.0001$, Kruskal-Wallis test.

(F). Representative images & quantification of γH2AX mean gray values in the indicated MEFs at 24 hours after direct irradiation (10Gy). DNA: Blue, γH2AX: Green (Scale bar: 35μm). The mean gray value of γH2AX in individual cell was measured as described in Methods. Values shown are median with interquartile range from two independent experiments with at least 200 cells analyzed per sample per experiment. ** $P \leq 0.01$, Kruskal-Wallis test.

Extended Figure 11.

E11A.

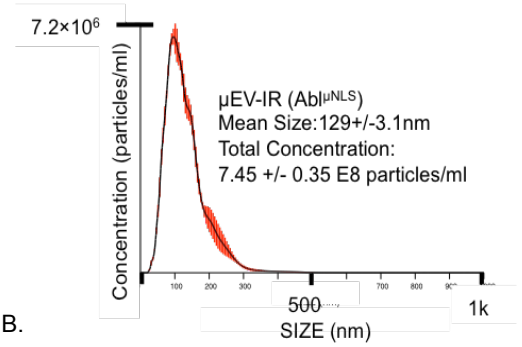

E11B.

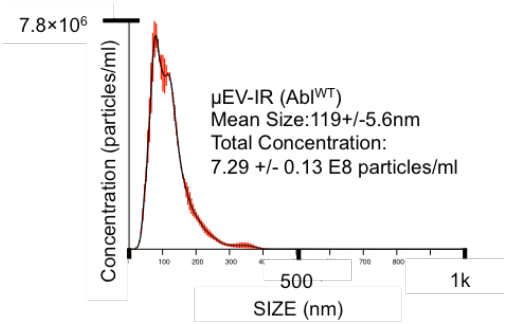

E11C.

E11D.

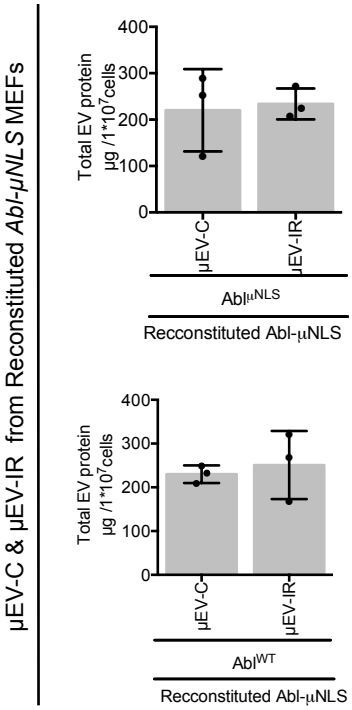

E11E.

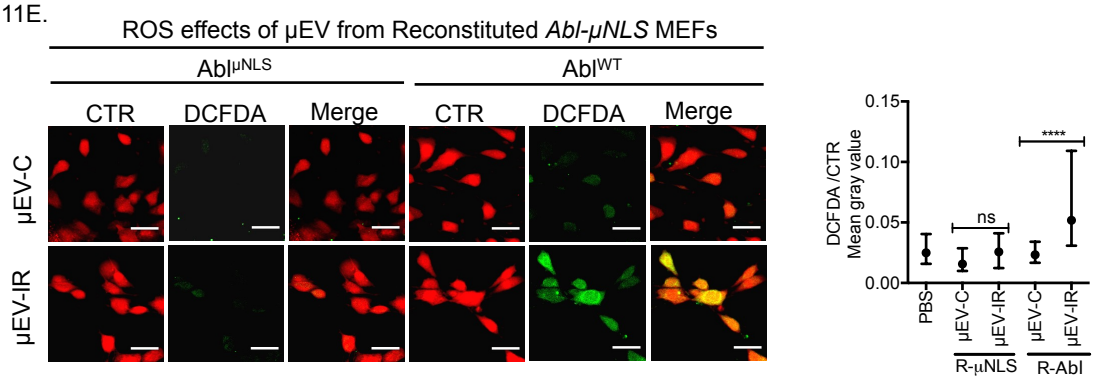

E11F.

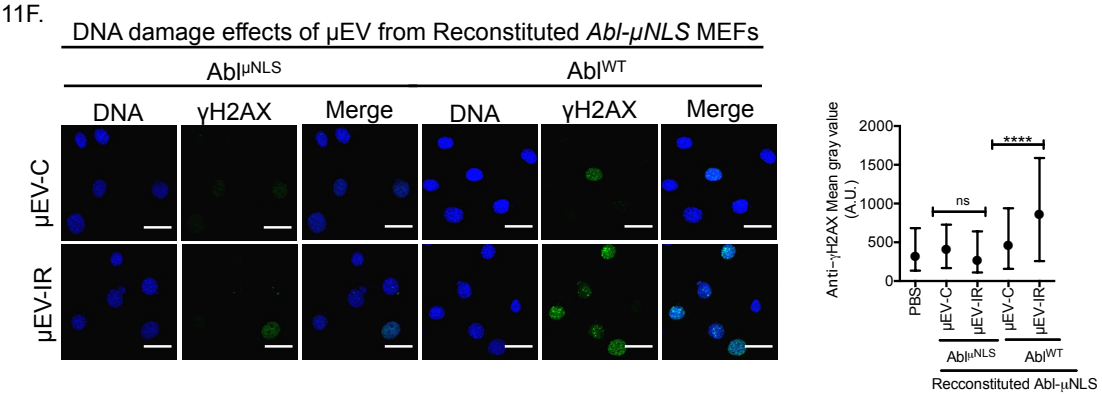

Extended Figure 11. Re-expression of Abl^{WT} but not $Abl^{\mu NLS}$ restored production of BE-Inducing μEV-IR

(A & B). Nanoparticle tracking analysis to determine the size distribution and concentration of particles in μEV-IR preparation isolated from media at 24 hours after irradiation (10Gy) of $Abl^{\mu NLS}$ & Abl^{WT} reconstituted *Abl-μNLS* MEFs.

(C & D). Total protein in μEV-C & μEV-IR. Values shown are mean ± SD from three independent EV preparations.

(E). Representative images & quantification of ROS: live responder cells treated with the indicated EV preparations (3.5μg each) were stained with Cell-tracker red (CTR) and DCFDA (green) at 24 hours after EV addition (Scale bar: 35μm). Values shown are ratios of DCFDA/CTR mean gray values as median with interquartile range from three independent experiments with at least 200 cells analyzed per sample per experiment. ns: not significant, ***$P \leq 0.001$, Kruskal Wallis test.

(F). Representative images & quantification of γH2AX mean gray values in responder cells treated with the indicated μEV-C & μEV-IR (3.5μg each) isolated from the reconstituted *Abl-μNLS* MEFs at 24 hours after EV addition. DNA: Blue, γH2AX: Green (Scale bar: 35μm). The mean gray value of γH2AX in individual cells was measured & shown as median with interquartile range from three independent experiments with at least 200 cells analyzed per experiment. ns: not significant, ****$P \leq 0.0001$,Kruskal-Wallis test.

Extended Figure 12.

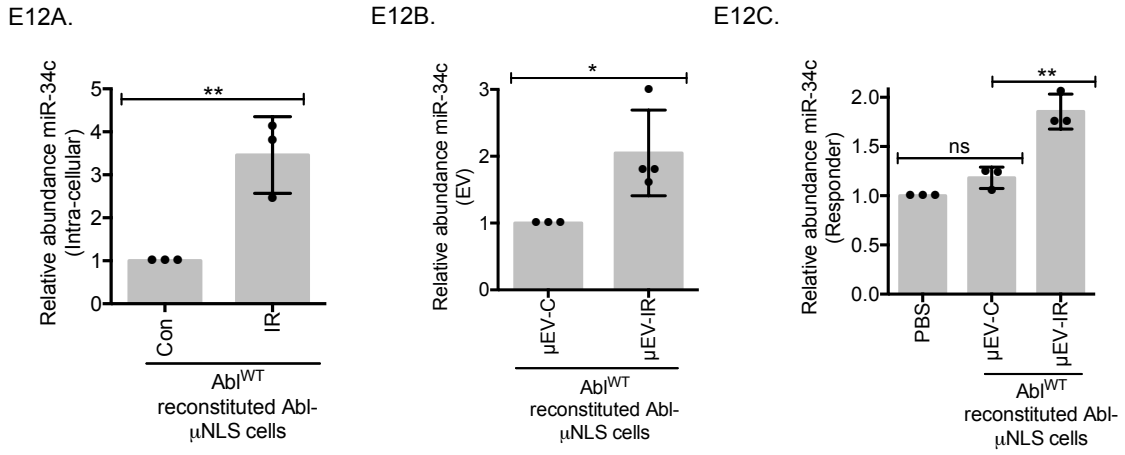

Extended Figure 12: Re-expression of Abl^{WT} in *Abl-μNLS* MEFs restored μEV-IR loading and transfer of miR-34c

(A). Intra-cellular levels of miR-34c in control & irradiated (10Gy) Abl^{WT}-reconstituted *Abl-μNLS* MEFs. U6-normalized miR-34c abundance in non-irradiated (Con) cells was set to 1. Values shown are mean ± SD from three independent experiments. ***P* ≤ 0.01, ONE WAY ANOVA.

(B). Relative abundance of miR-34c in EV preparations isolated at 24 hours after irradiation (10Gy) or not from Abl^{WT}-reconstituted *Abl-μNLS* MEFs. Values shown are relative abundance (mean ± SD) from three independent experiments. **P* ≤ 0.05, ONE WAY ANOVA.

(C). Relative abundance of miR-34c in responder cells treated for 24 hours with μEV-C & μEV-IR (25μg each) isolated from Abl^{WT}-reconstituted *Abl-μNLS* MEFs. Values shown are relative abundance (mean ± SD) from three independent experiments. ns: not significant, ***P* ≤ 0.01, ONE WAY ANOVA.

Extended Figure 13.

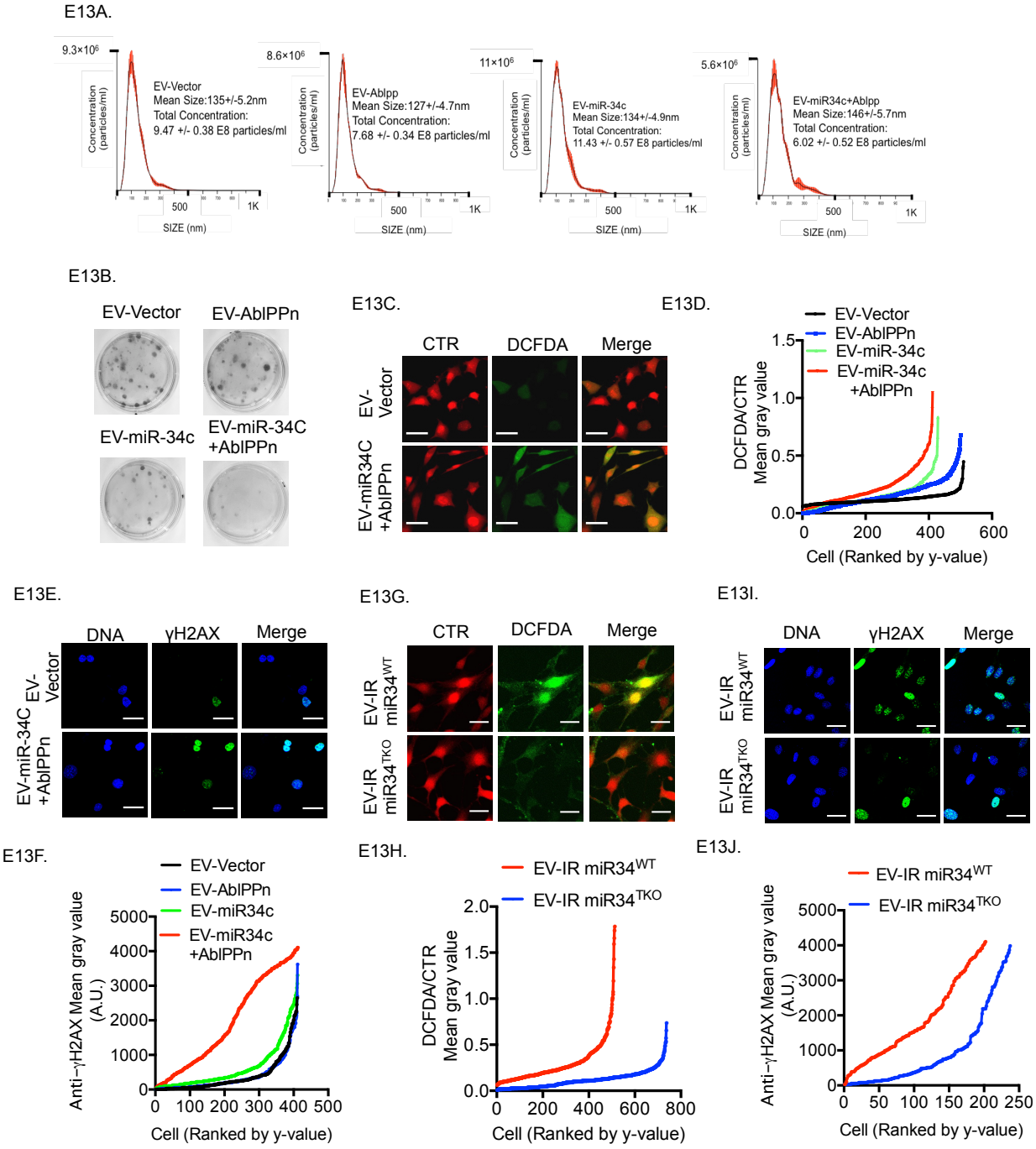

Extended Figure 13: Nanosight analyses of EV preparations from transfected HEK293T cells & representative images of bystander effects induced in responder MEFs

(A). Nanoparticle tracking analysis to determine the size distribution and concentration of particles in EV-Vector, EV-AblPPn, EV-miR-34c & EV-miR-34c+AblPPn isolated from culture media at 24 hours after transfection of HEK293T cells with the indicated plasmids.

(B). Representative images of colony formation in responder MEFs treated with EV-Vector, EV-AblPPn, EV-miR-34c & EV-miR-34c+AblPPn (25μg each). Quantification of results is shown in Fig. 4H.

(C). Representative images of live responder cells stained with Cell-tracker red (CTR) and DCFDA (green) at 24 hours after treatment with EV-miR-34c or EV-miR-34c+AblPPn (25μg each) (Scale bar: 35μm). Quantification of results is shown in Fig. 4I.

(D). The ratios of DCFDA/CTR mean gray values of individual cells from one experiment for Fig. 4I.

(E). Representative images of γH2AX staining in responder MEFs after 24 hours of treatment with EV-miR-34c or EV-miR-34c+AblPPn (25μg each), DNA: Blue, γH2AX: Green (Scale bar: 35μm). Quantification of results is shown in Fig. 4J.

(F). The γ-H2AX mean gray values of individual cells collected from one experiment for Fig. 4J.

(G). Representative images of live responder cells stained with Cell-tracker red (CTR), and DCFDA (green) after 24 hours of treatment with EV-IR (25μg each) isolated from media conditioned by 10Gy irradiated miR34^{WT} or miR34^{TKO} MEFs (Scale bar: 35μm). Quantification of results is shown in Fig. 4K.

(H). The ratios of DCFDA/CTR mean gray values of individual cells collected from one experiment for Fig. 4K.

(I). Representative images of γH2AX staining in responder MEFs after 24 hours of treatment with the indicated EV-IR (25μg each) preparations. DNA: Blue, γH2AX: Green (Scale bar: 35μm). Quantification of results is shown in Fig. 4L.

(J). The γ-H2AX mean gray values of individual cells collected from one experiment for Fig 4L.

Extended Figure 14.

E14A.

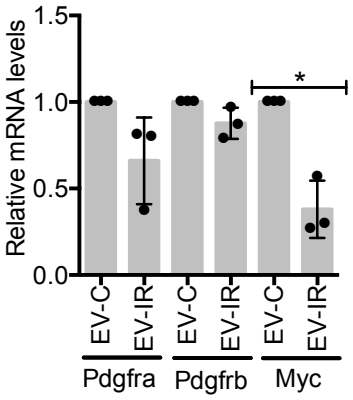

E14B.

Primer List: Sequence 5’ to 3’
U6-F: CTCGCTTCGGCAGCACA
U6-R: AACGCTTCACGAATTTGCGT
Stem-loop primer miR34C: GTCGTATCCAGTGCAGGGTCCGAGGTATTCGCACTGGATACGACGCAATC
q-miR34C-F: AGGCAGTGTAGTTAGCTG
q-miR-R: GTGCAGGGTCCGAGGT
p21-F: CCATGTGGACCTGTCACTGTCTT
p21-R: AGAAATCTGTCATGCTGGTCT
Pdgfrb1 F: GTTGTTGCTGTCCGTGTTATG
Pdgfrb1 R: GGCCCTAGTGAGTTGTTGTAG
Myc F: CGACTCTGAAGAAGAGCAAGAA
Myc R: AGCCAAGGTTGTGAGGTTAG
Pdgfra1 F: CTCAGAGAGAATCGGCCCCA
Pdgfra1 R: CACCAGCCTCCCGTTATTGT

Extended Figure 14: Levels of predicted miR-34c target genes in responder cells after treatment with EV-C or EV-IR

(A). Relative RNA levels for the indicated target genes in responder MEFs after treatment with EV-C (25µg) or EV-IR (25µg) for 24 hours. Values shown are relative RNA abundance (mean ± SD) from three independent experiments. *$P \leq 0.05$, ONE WAY ANOVA.

(B). List of primers used to quantify miR-34c and target gene RNA.